Shading Correction for Grating-based Differential Phase Contrast X-ray Imaging

Sebastian Kaeppler, Johannes Wandner, Thomas Weber, Andreas Maier,
Gisela Anton, Joachim Hornegger, Christian Riess

***Abstract*—Grating-based differential phase-contrast X-ray is a novel imaging modality with excellent soft-tissue contrast. Besides standard X-ray attenuation, it provides complementary information on the differential phase shift and the dark-field signal, which reveals structure variations at (sub-)micron scale. Current experimental setups suffer from a narrow field of view of 2-4cm. Thus, multiple exposures have to be stitched together to image larger objects. However, individual exposures are inherently affected by intensity variations, such that tiling artifacts corrupt the stitched projection. These artifacts are most severe in the differential phase image and highly impact their diagnostic value.**

To address this issue, we propose a novel optimization-based algorithm for fully compensating these tiling artifacts. Our algorithm estimates a smooth bias field for each individual exposure with a global objective function that minimizes the intensity distortion within and across different tiles in the projection. Compared to a currently widely used heuristic, our algorithm leverages the information available from all exposures to estimate the individual bias fields. The evaluation shows the superiority of the proposed algorithm, as it produces bias-free images. To our knowledge, this is the first bias correction algorithm for differential phase images that yields images with nearly imperceptible transitions between individual exposures.

***Index Terms*—X-ray, interferometry, grating, differential phase contrast, shading, artifact correction**

I. Introduction

Phase-sensitive X-ray imaging has the potential to provide soft-tissue contrast of unprecedented diagnostic value. Different measurement principles have been proposed to obtain phase-sensitive images. Most commonly used are propagation-based systems [1], diffraction-enhanced systems [2] and grating-based interferometers [3]. One particular benefit of grating-based systems is that three output images are obtained, containing complementary per-pixel information on absorption (i.e., overall intensity attenuation), differential phase-contrast (DPC) of the X-ray wavefront, and dark-field contrast (i.e., the contrast reduction of the grating pattern due to the object). The field of view of current experimental grating-based setups is limited to 2-4 centimeters due to the challenges in the grating manufacturing process. When imaging larger objects it is thus necessary to acquire multiple image tiles by translating the object perpendicular to the beam direction. After acquisition, these tiles are stitched together to form the full projection.

Unfortunately, the DPC images of individual exposures suffer from intensity inhomogeneities, which mainly arise from thermal effects and calibration inaccuracies. These inhomogeneities can lead to severe tiling artifacts in the stitched DPC images, which greatly hamper their interpretability and further processing. To our knowledge, there exists no published method on how to address this issue for stitched projections.

Tapfer et al. proposed a correction step for non-stitched DPC projections acquired for Phase Contrast Tomography [4]. This method uses the average image gradient in x- and y- direction to define a linear intensity plane for each DPC projection. The resulting plane is then subtracted from the DPC image. This approach often leads to suboptimal results when applied to data acquired for stitched projections, for two reasons. First, it can be observed that DPC bias fields may be more complex for a linear plane model. Second, this method does not utilize the information available from adjacent exposures. This may on one hand lead to a more accurate estimate of the true bias field, but comes at the expense of inter-tile artifacts. Additionally, DPC tomographic data capturing is typically designed to cover the whole object within the field of view to avoid truncation artifacts. Having large portions of air at the image boundaries eases the estimation of the bias field. However, the projections acquired for stitching may not contain any air. Hence, this planar approach is prone to variations in image content, while not fully utilizing prior information on the stitching geometry. Due to these shortcomings, stitched projections processed with this approach oftentimes still exhibit residual tiling artifacts.

In this paper, we propose a method for shading correction for stitched DPC images that addresses these issues. Our method uses truncated radial basis functions to model an additive bias field that is smooth within each individual exposure, but still can be discontinuous between adjacent tiles. Our method seeks to minimize sharp transitions between individual tiles, as those are a strong indicator of a bias field, while also promoting sparseness of the resulting DPC image to support homogeneity within individual exposures.

II. Methods

Two design choices have to be made when performing bias correction: the parameterization of the bias field and the cost function that determines its estimation. Our method uses a local parameterization for each exposure, with a global cost function to estimate these parameters. For each tile $\boldsymbol{t}$ consisting

S. Kaeppler, A. Maier, J. Hornegger and C. Riess are with the Pattern Recognition Lab, Department of Computer Science, Friedrich-Alexander-University Erlangen-Nuremberg, Erlangen, Germany.

J. Wandner, T. Weber and G. Anton are with the Erlangen Centre for Astroparticle Physics, Deparment of Physics, Friedrich-Alexander-University Erlangen-Nuremberg, Erlangen, Germany.

Corresponding author: Sebastian Kaeppler, sebastian.kaeppler@fau.de

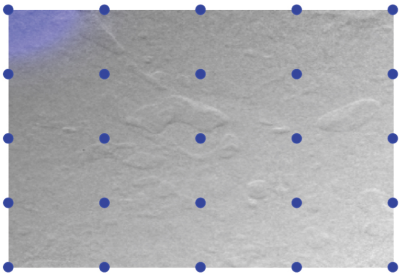

Fig. 1: Illustration of the positions of the radial-basis functions for one tile with $n = 5$. The center of each basis function is given by the blue circles, while the support of the first basis function is shown by the blue shading.

of $s_\mathrm{x} \times s_\mathrm{y}$ pixels, we parameterize the additive bias field by a set of $n \times n$ Gaussian radial basis functions. Each basis function is determined by its center position $\boldsymbol{c}_{i,j} = (c^\mathrm{x}_{i,j}, c^\mathrm{y}_{i,j})$, a scaling factor $v_{i,j}$, and standard deviation σ. The basis centers $\boldsymbol{c}_{i,j}$, $1 \leq i, j \leq n$ are placed on an equidistant grid over the tile, such that the outer-most functions reside on the edges and corners of the tile (see illustration in Fig. 1). The standard deviation σ of all functions is chosen uniformly and fixed as

$$\sigma = 0.25 \cdot \left(\frac{s_\mathrm{x}}{n-1} + \frac{s_\mathrm{y}}{n-1} \right) \quad . \tag{1}$$

The set of basis functions defines a local bias field $\boldsymbol{b}$. At pixel position (x, y) the intensity of the local bias field is given by

$$\boldsymbol{b}(x,y) = \frac{\sum_{i,j} v_{i,j} \cdot e^{-\left(\frac{(x-c^\mathrm{x}_{i,j})^2}{2\sigma^2} + \frac{(y-c^\mathrm{y}_{i,j})^2}{2\sigma^2} \right)}}{\sum_{i,j} e^{-\left(\frac{(x-c^\mathrm{x}_{i,j})^2}{2\sigma^2} + \frac{(y-c^\mathrm{y}_{i,j})^2}{2\sigma^2} \right)}} \quad . \tag{2}$$

Within the tile, $\boldsymbol{b}(x, y)$ evaluates to a smooth function because the basis functions overlap. At tile borders, the support of the basis functions is truncated to allow discontinuities in the global bias field between adjacent tiles.

To obtain the bias field, the scaling factors $v_{i,j}$ are estimated for all tiles simultaneously (the center locations $\boldsymbol{c}_{i,j}$ and the standard deviation σ are constant). The objective function for the estimation is designed to promote homogeneity within each tile and penalizes discontinuities between adjacent tiles, i.e.,

$$\arg\min_{\boldsymbol{V}} \frac{\|\boldsymbol{I} - \boldsymbol{B_V}\|_1}{\#\mathrm{pixels}} + \alpha \cdot \frac{\|\nabla_\mathrm{border}(\boldsymbol{I} - \boldsymbol{B_V})\|_2}{\#\mathrm{borderpixels}} \quad . \tag{3}$$

Here, $\boldsymbol{V}$ denotes the scaling factors of all basis functions over all tiles, $\boldsymbol{I}$ denotes the pixel intensities of the stitched input DPC image and $\boldsymbol{B_V}$ is the global bias field defined by $\boldsymbol{V}$. The first term promotes sparsity of the resulting images through use of the L_1 norm. For differential images, sparsity can be used as a measure of homogeneity, as inhomogeneities lead to an increased number of non-zero intensities. The second term captures discontinuities at tile borders. The gradient operator ∇_border yields the gradient of the image in stitching direction at tile borders, while being zero for all other locations. Each term is normalized by the respective pixel count. The scaling parameter α is used to balance both terms. The resulting objective function is minimized using the Broyden-Fletcher-Goldfarb-Shanno (BFGS) method [5] until convergence. Finally, the estimated bias field $\boldsymbol{B_V}$ is subtracted from the DPC image.

III. Experiments and Results

For evaluation, we compared our proposed algorithm to the planar correction model. We performed a quantitative evaluation using a wedge phantom. We also qualitatively compared the results on various biological specimens. All images were acquired using our experimental setup of a three-grating Talbot-Lau interferometer, as reported in [6]. Each tile had a size of 360×360 pixels. The parameters for our algorithm were determined using pilot experiments on separate data. We set the number of basis functions $n = 5$ and $\alpha = 50$.

For the quantitative evaluation, we acquired DPC images of a PMMA wedge phantom surrounded by air. The wedge is located in the bottom left of the images in Fig. 2, and stretched over three tiles. For the pixels inside the wedge, we computed the standard deviation of the intensities. Since the slope of the wedge is constant, the ground truth standard deviation is 0. Experimentally, we obtained a standard deviation of 0.0566 for the raw data, 0.0172 for the planar approach and 0.0155 for the proposed method. For the remaining image pixels, corresponding to air, we also computed the standard deviation and, additionally, the mean of the intensities. Both should be 0 in ideal DPC signals. In this experiment, we obtained a mean and standard deviation of 0.162 ± 0.0652 for the raw data, 0.0054 ± 0.0167 for the planar method and 0.0018 ± 0.0123 for the proposed approach. For both measurements, the proposed method performs considerably better. These results are also in line with the visual impression of the resulting images. In Fig. 2(d), we show on the y-axis the intensity variations for all three approaches along the annotated lines in the images. It shows that the proposed method (red) indeed leads to the most homogeneous result. For an additional qualitative evaluation, we applied the proposed algorithm to images of biological specimens, acquired by our group. For all specimens, we observed similar performance in the correction of inter-tile artifacts. The DPC shading artifacts were invisible in all data sets after processing with our algorithm. A representative sample result, obtained for an ex-vivo dissected human breast, is shown in Fig. 3, together with a comparison with the planar approach.

IV. Discussion and Conclusions

In this paper, we presented a novel algorithm for correcting tiling artifacts in stitched differential phase contrast images obtained with grating-based X-ray interferometry. To our knowledge, this problem has up to now not been addressed in the literature. We globally optimize a non-linear bias field that promotes intra-tile smoothness while allowing inter-tile discontinuities, to maximize sparsity and minimize transitions at tile borders. In the evaluation, the proposed approach yields almost perfect artifact correction in cases where the simpler planar approach fails.

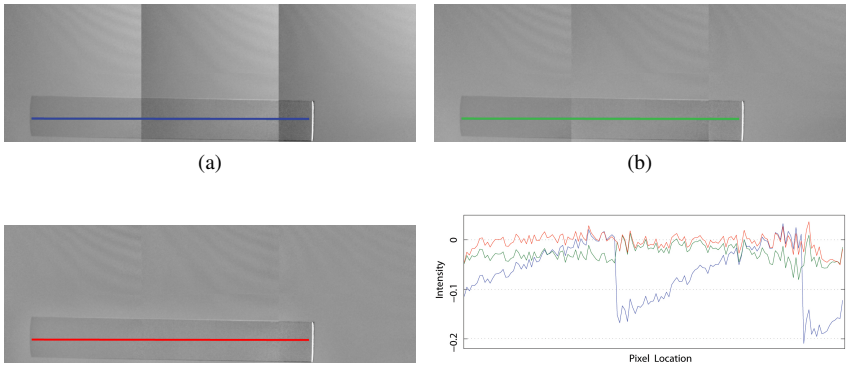

(a) (b) (c) (d)

Fig. 2: DPC images of the used phantom with line profiles. (a) Raw data. (b) Planar shading correction. (c) Proposed shading correction. (d) Line profiles along the wedge phantom. The proposed method (red) leads to the most homogeneous result.

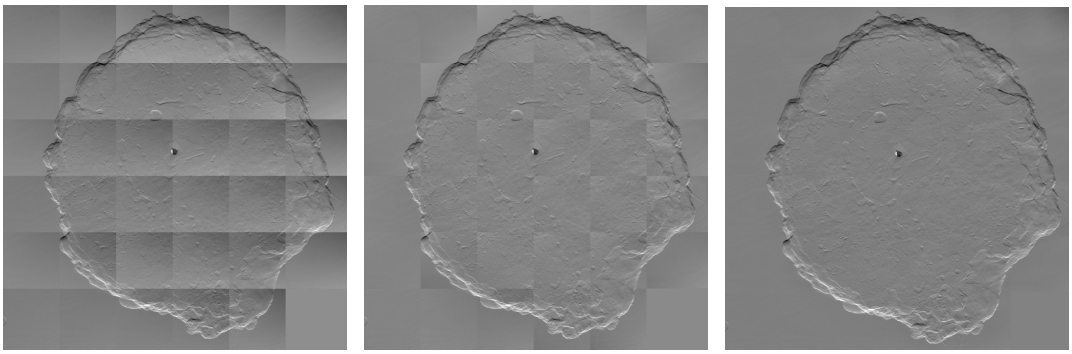

(a) (b) (c)

Fig. 3: DPC image of an ex-vivo human breast. (a) Raw data. (b) Planar shading correction. (c) Proposed shading correction. Note that the residual shading in (b) is non-planar.

In future work, improvements on the algorithm run time can be investigated by exploiting potential similarities in the bias field for adjacent tiles. Also, a physically motivated parameterization of the bias field can be considered. Finally, to a much lesser extent, the dark-field image is also affected by tiling artifacts, for which this algorithm could potentially be adapted.

ACKNOWLEDGMENTS

This work was funded by the German Ministry for Education and Research (BMBF), project grant No. 13EX1212B and the cluster of excellence Medical Valley EMN and Siemens Healthcare. The authors acknowledge support from the Research Training Grant 1773 by the German Research Foundation. The authors thank Dr. Jürgen Mohr and Jan Meiser from the Karlsruhe Institute of Technology and the Karlsruhe Nano Micro Facility (KNMF) for manufacturing the gratings used in the experiments and the University Hospital of Erlangen for providing the breast specimen.

REFERENCES

[1] S. W. Wilkins, T. E. Gureyev, D. Gao, A. Pogany, and A. W. Stevenson, "Phase-contrast imaging using polychromatic hard x-rays," *Nature*, vol. 384, no. 6607, pp. 335–338, Nov. 1996.

[2] C. Parham, Z. Zhong, D. M. Connor, L. D. Chapman, and E. D. Pisano, "Design and implementation of a compact low-dose diffraction enhanced medical imaging system," *Academic Radiology*, vol. 16, no. 8, pp. 911–917, Aug. 2009.

[3] F. Pfeiffer, T. Weitkamp, O. Bunk, and C. David, "Phase retrieval and differential phase-contrast imaging with low-brilliance x-ray sources," *Nature Physics*, vol. 2, no. 4, pp. 258–261, Apr. 2006.

[4] A. Tapfer, M. Bech, A. Velroyen, J. Meiser, J. Mohr, M. Walter, J. Schulz, B. Paulwels, P. Bruyndonckx, X. Liu, A. Sasov, and F. Pfeiffer, "Experimental results from a preclinical x-ray phase-contrast ct scanner," *Proceedings of the National Academy of Sciences*, vol. 109, no. 39, p. 1569115696, 2012.

[5] R. Fletcher, *Practical Methods of Optimization*. John Wiley & Sons, Inc., 1987.

[6] T. Michel, J. Rieger, G. Anton, F. Bayer, M. Beckmann, J. Durst, P. Fasching, W. Haas, A. Hartmann, G. Pelzer, M. Radicke, C. Rauh, A. Ritter, P. Sievers, R. Schulz-Wendtland, M. Uder, D. Wachter, T. Weber, E. Wenkel, and A. Zang, "On a dark-field signal generated by micrometer-sized calcifications in phase-contrast mammography," *Physics in Medicine and Biology*, vol. 58, no. 8, pp. 2713–2732, Apr. 2013.